

# Seismic Fragility Analysis of a RC Bridge with Uniform and Non-Uniform Random Scour Patterns

Ali Raof Mehrpour Hosseini <sup>a</sup>, Mehran S. Razzaghi <sup>a,\*</sup>, Nasser Shamskia <sup>a</sup>

<sup>a</sup>Department of Civil Engineering, Qazvin Branch, Islamic Azad University, Qazvin, Iran

Received 25 October 2023, Accepted 27 February 2024

## Abstract

Previous natural disaster assessments had identified bridges as vulnerable structures against hydraulic hazards, particularly scouring. Additionally, in areas with high seismic activity, bridges are exposed to minor damage to complete collapse, in most cases requiring immediate occupancy structural performance levels in the event of an earthquake. Previous studies have focused on vulnerability assessments by considering the effects of simultaneous hazards. This study examines a simply supported RC bridge model with a discontinuous deck-girder superstructure installed on cap beams via elastomers. Seismic vulnerability assessments were conducted by developing fragility curves through nonlinear time history analyses on scoured models. One of the study's objectives is to consider the effects of non-uniform patterns in different foundations of the four-span model by generating random depth samples. The study also evaluated even depths as the uniform scenario for vulnerability assessment. The results indicate that, in all limit states considered in the study, the uniform has a higher probability of exceeding the limit states than the non-uniform scenario. However, in evaluating critical scoured models, the uniformly maximum credible scoured pattern did not necessarily have a higher probability of exceeding all limit states. In other words, the non-uniform scenario, which had pier(s) with the maximum credible scour depth, had a more critical vulnerability in some limit states.


**Keywords:** Bridge; Fragility analysis; Scour; Multi-hazard; Vulnerability assessment.

## 1. Introduction

The bridge is a crucial transportation component and is particularly important in vulnerability assessments. Climate change and frequent flooding have resulted in significant economic losses, particularly in recent decades. One consequence of flooding is the scour occurrence in the foundation of bridge substructures [1]. Scouring is the material removal from the soil bed of channels and riverbeds due to water interactions [2]. This removal reduces the foundation's capacity and, subsequently, the entire structure's capacity by altering the support conditions. Furthermore, scouring affects the structure's dynamic characteristics and may act as a seismic isolator, reducing the effect of changes in foundation capacity [3]. To understand the mechanism and function of scouring, several studies have monitored this phenomenon in bridge foundations using sensors and instruments [4-7]. Many researchers have considered scouring an inevitable occurrence in their study cases.

Additionally, the results obtained from these studies, which examine the factors affecting scouring, have been beneficial in providing estimation relationships for scour depth.

In contrast to other types of structures, bridges possess a considerable mass at their upper portion and are evaluated differently in terms of their ability to withstand seismic loads. Previous earthquakes, such as the Kobe and Northridge earthquakes, have demonstrated that these structures can suffer from minor damage or even collapse. To evaluate the incidents and resulting damages caused to bridges, several studies have been conducted. Priestley [8], Mitchell et al. [9], and Chang et al. [10] conducted field investigations after the Whittier Narrows, Northridge, and Chichi events, respectively. Additionally, Lehman et al. [11], Saedi et al. [12], and Su et al. [13] assessed the performance of laboratory models ranging from small to large scale.

 \*Corresponding Author: Email Address: razzaghi.m@gmail.com

Vulnerability is a highly efficient aspect of risk assessment that reveals the extent to which a structure is susceptible to damage [14]. Such evaluations are ultimately useful in predicting the potential damages that may result from a given hazard, as well as in developing retrofitting plans and making economic decisions. Fragility curves are a valuable tool in vulnerability assessments, and several studies have developed such curves for hydraulic-related damages [15-17]. However, the vulnerability assessment against seismic loads, particularly in the aftermath of the San Fernando and Loma Prieta earthquakes, has drawn significant attention to the vulnerability of highway bridges [18]. Numerous studies have developed earthquake fragility curves for bridges, considering various factors [19-24].

The interaction of multiple hazards can change the performance of a structure, which has motivated many researchers to conduct multi-hazard assessments in recent years [25-28]. Bridges are highly vulnerable to earthquakes and scouring. Therefore, several studies have evaluated the simultaneous effects of these two hazards [29-33]. Alipour and Shafei [34] conducted a vulnerability assessment on two-span and three-span bridge models, considering scouring scenarios ranging from zero to five meters deep and uniformly at the foundations. The fragility curves developed in this study indicate an increase in vulnerability with increasing scour depth in minor and moderate limit states. Alipour et al. [35] conducted a reliability assessment on a set of nine two-span bridges crossing over two rivers with low- and high-flow discharge rates. Guo et al.'s study [36] performed fragility analyses on two models of two-span and three-span uniformly scoured box-girder bridges. This study developed time-dependent fragility surfaces, and the results generally show an increase in vulnerability during the longer service life of the bridge.

Many other studies have been conducted on bridges with two or more spans, where the uniform scour depth has been considered. However, due to the uncertainties in the formation of cavities resulting from soil erosion around the foundation of various bridge bents, this study has taken into account the scour depth randomly and, in some cases, non-uniformly. To make comparisons, random depths have also been applied uniformly to the foundations, and seismic fragility curves have been developed to compare various scouring scenarios.

## 2. Scour Estimation

### 2.1. Probabilistic Scour Hazard Analysis

Numerous researches have been conducted previously to estimate the extent of erosion in soils that are either sandy or cohesive [37-40]. Given that the primary objective of this study is to examine the random effect of erosion, it is imperative to establish a probabilistic framework for estimating the depth of scour. Consequently, the current study utilized the equation proposed by Johnson and Dock [41]. The methodology of this equation is founded on acknowledging the uncertainty in the relationship suggested by Richardson and Davis [37]. The formulation of this equation is as follows:

$$y_s = 2.0\lambda_{sc}y_0K_sK_\theta K_3K_4\left(\frac{d_p}{y_0}\right)^{0.65}F_r^{0.43} \quad (1)$$

In this equation, the variable  $y_s$  represents the scour depth, while  $\lambda_{sc}$  is the correction factor proposed by Johnson and Dock [41].  $d_p$  refers to the diameter of the pier,  $y_0$  represents the depth of flow just upstream of the foundation, and  $F_r$  is the Froude number. Additionally,  $K_s$ ,  $K_\theta$ ,  $K_3$ , and  $K_4$  are correction factors depending on the nose shape of the pier, the angle of the flow's attack, the conditions of the stream bed, and the size of the river bed material.

Given that there have been no studies conducted on the probabilistic distribution of  $K_s$  and  $K_4$ , these factors have been used as deterministic variables in the equation. The circular shape of the sections has led to the assumption that the  $K_s$  factor is equal to 1.0. In this study, the bed material was assumed to be medium sand, as sand is more erosive than cohesive materials. Since  $K_4$  is dependent on the size of the bed material, it has been considered equal to 1.0.

If we assume that the direction of the river flow is perpendicular to the piers, then the value of factor  $K_\theta$  is equal to 1.0. However, during a flood, the angle of attack may change depending on the flood conditions. Therefore, in this study, it is assumed that the factor follows a normal distribution with a mean of 1.0 and a coefficient of variance (COV) of 0.05. Assuming a plane bed condition, the value of  $K_3$  can be determined to be equal to 1.1. Generally, it is very challenging to estimate the bed condition, especially during a flood. This parameter also

follows a normal distribution with a mean of 1.1 and a COV of 0.05. [3, 41, 42].

One can determine the flow depth, represented as  $y_0$ , by utilizing the flow discharge rate  $Q$  and applying the hydraulic relationship provided in equation (2).

$$Q = \frac{by_0}{n} \left( \frac{by_0}{b + 2y_0} \right)^{0.67} S^{0.5} \quad (2)$$

In the given equation, the variable  $b$  represents the width of the river bed,  $n$  is the Manning roughness coefficient, and  $S$  refers to the slope of the bed stream. For this study, the value of  $S$  has been assumed to be 0.002, which is consistent with the values used in several previous studies and indicates a relatively gentle slope of the bed [3]. The correction factor for scour modeling, denoted by  $\lambda_{sc}$ , varies depending on the conditions of the bridge site. Various distributions are available for this factor. In the present analysis, assuming a medium sand condition, a triangular distribution with a mean of 0.93, a lower limit of 0.8, and an upper limit of 1.0 has been used [41].

The Manning roughness coefficient, evaluated in previous studies, is considered to have a lognormal distribution with a mean of 0.025 and a COV of 0.275 [34]. Additionally, the parameter  $b$  used in the equation is assumed to be equal to the bridge's total length, as detailed information about the investigated river is not available. This assumption is similar to other studies, such as Wang et al. [3].

The equation used takes into account the discharge as a random variable. Research studies have utilized the lognormal distribution to calculate the discharge [34]. The scouring analyses were based on the annual peak discharge data of a river in Iran, which was obtained from the Iran Water Resources Management Company.

In this study, the scour depth estimation has been carried out probabilistically by utilizing the provided equations and considering the relevant random variables for flood events with a 100-year return period. The selection of this return period aligns with the guidelines outlined in Aashto [43] for bridge design criteria requirements concerning scour. To generate the probabilistic scour hazard curve 100,000 simulations were conducted using the Monte Carlo technique, as illustrated in Fig. 1.

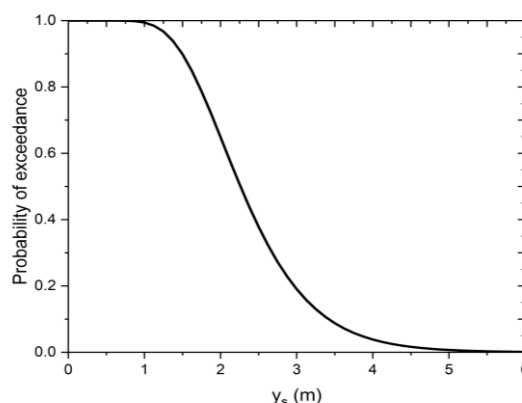


Fig. 1. Probabilistic hazard curve of the bridge according to the river discharge data

Based on the scour hazard curve calculation, a scour depth of 3.84 meters can be obtained if a probability of 5% is considered. However, in this study, probability values less than 5% were assumed to be insignificant. Therefore, the maximum credible scour depth, a widely used parameter in this study, has been determined as a depth equivalent to 4 meters.

## 2.2. Random Scour Patterns

In the previous analysis stage, simulations were created using the Monte Carlo technique. However, the number of simulations generated was too large to be modeled in structural analysis. In this study, the Latin hypercube sampling technique was utilized to select several random depths based on the probability intervals presented in Fig. 1. These random depths were assigned to different foundations using this technique, resulting in non-uniform patterns. The main objective of this study is to evaluate the impact of uneven scour depths on the bridge's different foundations. Random depths were also employed to generate uniform patterns with the same washed-out depth in distinct foundations. By assigning these patterns to the structural model and conducting seismic analysis, it is possible to assess the multi-hazard effects of earthquake and scour for the non-uniform and uniform conditions.

## 3. Case Study

### 3.1. Bridge Description

The main goal of the current study is to assess the susceptibility of a reinforced concrete (RC) bridge

that is commonly used in Iran. To achieve this objective, the researchers utilized the bridge model from Mosleh et al.'s study [44] for their analysis. The bridge model is a multi-span simply supported RC bridge with a non-continuous superstructure that includes a deck-girder system supported by elastomers on the substructure. The total length of the bridge model is 79.2 meters, with four spans of 15.6, 24, 24, and 15.6 meters, respectively, and a width of 11.95 meters. Each bent of the bridge has three columns that are connected to a cap beam at the top, and seat-type abutments are used on each side of the bridge. The columns are circular with a diameter of 1.1 meters and a height of 6 meters, and they contain thirty 22mm longitudinal bars that are confined by 12mm spiral hoops with 250 mm spacing. The bridge also includes an integrated pile cap under the bents, which is connected to six circular reinforced concrete piles with a diameter of 1.2 meters and a height of 20 meters. The pile section contains 40 longitudinal bars with a diameter of 22 mm. The expansion joint between the deck and the abutment is 50 mm, and the expansion joint between the superstructure elements is 100 mm. The specific compressive strength of concrete in girders is 28 MPa, and in other members, it is 24 MPa. All the reinforcements used in the bridge are considered to have a yield strength of 400 MPa and an ultimate strength of 600 MPa.

### 3.2. Modeling

The geometry was precisely modeled in three dimensions and six degrees of freedom using the OpenSees software, an open-source framework for finite element analysis of structure and soil [45]. The superstructure, which includes the deck and girders, was defined using equivalent elastic beam-column elements. All columns and piles were modeled using displacement beam-column elements known as elements with distributed plasticity. The cross-section of these elements was constructed utilizing the fiber command, which consists of confined and unconfined concrete patches along with a circular layer of steel. The modeling of the concrete materials used in these sections was done using Concrete07, and the confinement effects were considered following the study by Mander et al. [46]. Additionally, the reinforcements have been defined using ReinforcingSteel materials. It is necessary to mention that the nodes determining the columns were spaced at intervals of 0.25 meters at

the top and bottom and 0.5 meters along the middle two meters of the column. The nodes defining the pile element were spaced at intervals of 0.25 meters. Elastic beam-column elements were used to model other members, such as the cap beams, pile caps, and abutments. In this study, the abutments were simulated as rigid blocks. Specifically, the nodes that make up the abutment were designed to generate the surface of an equivalent block. Similarly, the nodes of soil behind the abutment were also modeled, except that all degrees of freedom in the backfill nodes were assumed to be fixed. The passive behavior of the backfill-abutment system was defined using the hyperbolic force-deformation behavior model. To incorporate this hyperbolic behavior into the finite element model nonlinear zero-length compression-only springs with the HyperbolicGapMaterial function were utilized. One end of the zero-length spring was connected to the rigid block node that was equivalent to the surface of the abutment while the other end was connected to the corresponding fixed node that was equivalent to the backfill [47]. In bridge abutments, shear keys were also modeled as lateral supports to transfer the horizontal reactions of the superstructure to the abutments. This was accomplished by using zero-length elements that incorporated hysteretic behavior [48,49].

Elastomers exhibit significant resistance to gravity loads and transfer horizontal loads to the substructure through friction. It means that the behavior of the elastomer is determined by its stiffness, as long as the friction force between the elastomer and the concrete can support the incoming horizontal load. However, if the horizontal load exceeds the friction resistance, the stiffness of the elastomer becomes zero, resulting in behavior similar to complete elastoplastic behavior. To define the behavior of this element, Steel01 material has been used. According to CALTRANS [50], the coefficient of friction between concrete and elastomer is 0.4. The values of elastomer properties, including vertical stiffness ( $K_v$ ), shear stiffness in piers ( $K_s$ ), and shear stiffness of the abutments in the longitudinal ( $K_{al}$ ) and transverse ( $K_{at}$ ) directions, have been assigned as 695, 2.53, 10.14, and 22.94  $\frac{kN}{mm}$ , respectively.

The impact element is a crucial factor in the behavior of bridge models, particularly in the class of simply supported bridges with expansion joints. One potential cause of damage in these bridges is the

pounding between the superstructure elements and between the superstructure elements and the bridge abutments. Impact elements are only activated when the expansion joints are closed due to lateral excitation. Muthukumar [51] suggested a bilinear inelastic behavior model to describe the impact between elements. This model involves defining zero-length elements between the corresponding nodes of the superstructure and superstructure-abutment based on the expansion gaps.

This study investigates the scouring effect by considering the definition of soil-pile interaction behavior in modeling. This behavior was defined by using p-y, t-z, and q-z springs, which respectively represent the lateral resistance, axial friction, and bearing resistance of the pile tip, as the interface between the soil and the pile as a zero-length element. The force-deformation curve in p-y springs was calculated according to the method proposed by API [52], considering medium sand. The t-z behavior curve of the spring was obtained from the approximate Mosher relation [53] by calculating the ultimate side friction axial resistance from the Kulhawy method [54,55]. Finally, the behavior of the q-z springs was determined based on Vijayvergiya's approach [56]. The ultimate bearing resistance of the pile tip was defined using the Meyerhoff relation [57,58]. It is important to note that p-y and t-z springs were defined at the interface of corresponding pile and soil nodes with a distance of 0.25 meters using zero-length elements, and the scouring effects were applied to the structure by removing these springs depending on the considered scour depth. The geometry of the bridge model and the behavior curve of the materials used are depicted in Fig. 2.

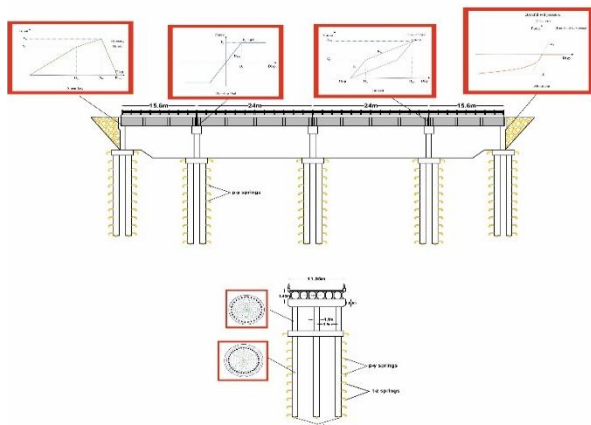


Fig.2. Schematic illustration of longitudinal and transverse views of the bridge model

### 3.3. Model Verification

A nonlinear time history analysis was conducted to validate the model. The model was subjected to an analysis of the two horizontal components of the Manjil Abbar earthquake record with a moment magnitude of  $M_w=7.6$ . This earthquake record was previously used in a study by Mosleh et al. [44]. In that study, concentrated plastic hinges were used in column finite element modeling employing Sap 2000 software. However, the study did not consider the modeling of soil-structure interaction and the effects of scouring. Therefore, restraints were created at the bottom of the columns in OpenSees software to verify the study. The displacement time history diagram of the second column in the longitudinal direction of the bridge is presented in Fig. 3. The results indicate a 9% difference between the response of the maximum column displacement in the two studies.

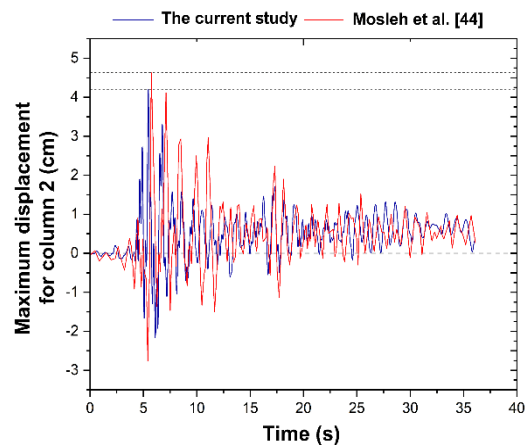


Fig. 3. A comparison of the displacement response of column 2 from the current study and from Mosleh et al. [44]

### 3.4. Response History Analysis

The study used nonlinear response history analyses (NRHA) to examine the seismic performance of the bridge model with uniform and non-uniform scour patterns, generated by the Latin hypercube technique. The study then assessed the vulnerability of the bridges using fragility analyses, which are probabilistic methods that estimate the conditional probabilities of a bridge reaching or exceeding a certain damage level under a given ground motion intensity [59]. These analyses help to understand the likelihood of bridge damage during an expected earthquake. The appropriate limit state in fragility

analysis is essential. Various studies have recommended different damage states, such as drift ratio, displacement ductility ratio, and strain-based criteria, which have advantages and disadvantages depending on the problem condition [20, 60, 61]. Some studies, such as Wang et al. [3], claim that drift ratio and displacement ductility ratio are not suitable for evaluating models under scour conditions. This is because scouring increases the foundation flexibility and causes higher vulnerability estimates based on total displacements using these damage states.

This study compares the peak strain in critical sections of columns and piles with the limit states determined by Kowalski [62] according to Table 1. The study defines two limit states for concrete bridges, which are serviceability and damage control, by considering concrete compression strain and steel tension strain as capacity criteria. Considering the consistent level of conservatism of the energy balance approach, it can be reasonably stated that concrete failure occurs until the compression strain level increases by at least 50% over the damage control limit strain [62]. Therefore, this limit state can be regarded as a standard for the ultimate limit state. The limit states are defined qualitatively as follows: The serviceability/minor indicates that “The bridge generally does not require structural repair but a cosmetic repair may be required”. The damage control/moderate limit state means that “The bridge requires structural repair”. Furthermore, the ultimate/extensive indicates that “The bridge has collapsed or suffered from

considerable damage that it is not feasible to repair” [62,63].

Table 1  
Limit state definition [62,63]

Damage state	Concrete strain limit	Steel strain limit
Serviceability/Minor	0.004(Compression)	0.015(Tension)
Damage control/Moderate	0.018(Compression)	0.060(Tension)
Ultimate/Extensive	0.027(Compression)	-

The study used cloud analysis (CA) to create fragility functions from nonlinear time history analyses. This technique has several advantages over other methods like incremental dynamic analysis (IDA), such as utilizing unscaled records with different intensity measures and distances from the source. This reduces the number of analyses, the uncertainties from the input motions, and the computational effort needed to develop the fragility curves [64,65]. The study selected 40 strong ground motions with dip-slip and strike-slip faulting mechanisms and a moment magnitude ( $M_W$ ) ranging from 6 to 7.5. The study also considered soil profiles with an average shear wave velocity ( $v_{s30}$ ) between 175 and  $375(\frac{m}{s})$ . The ground motions covered near-field and far-field distances. Tables 2 and 3 show the details of the ground motions used in the structural analyses. The study applied both horizontal components of the record to the bridge model in the nonlinear time history analysis. The study randomly assigned the larger component to the longitudinal or transverse direction of the bridge.

Table 2  
The list of selected ground motions with dip-slip faulting mechanism

Record	Magnitude ( $M_w$ )	Year	PGA(g)	$S_a(T_1)$ (g)	PGV( $\frac{m}{s}$ )	PGD(m)	$v_{s30}$ ( $\frac{m}{s}$ )	$R_{jb}$ (Km)	$R_{RUP}$ (Km)
Taiwan Smart(45)-O07	7.3	1986	0.16	0.38	0.23	0.09	314.33	54.17	54.17
N.Palm Springs-Palm Springs Airport	6.1	1986	0.19	0.24	0.13	0.03	312.47	10.08	10.84
Loma Prieta-Capitola	6.9	1989	0.51	0.59	0.38	0.07	288.62	8.65	15.23
Tabas-Boshrooyeh	7.4	1978	0.11	0.20	0.15	0.08	324.57	24.07	28.79
Taiwan Smart(45)-I07	7.3	1986	0.12	0.35	0.27	0.10	309.41	55.82	55.82
Coalinga-Cantua Creek School	6.4	1983	0.29	0.43	0.26	0.10	274.73	23.78	24.02
Taiwan Smart(45)-C00	7.3	1986	0.15	0.36	0.30	0.10	309.41	56.01	56.01
Coalinga-Pleasant Valley	6.4	1983	0.60	0.77	0.61	0.22	257.38	7.69	8.41
Gazli-Karakyr	6.8	1976	0.86	0.91	0.68	0.27	259.59	3.92	5.46
N.Palm Springs-North Palm Springs	6.1	1986	0.69	0.87	0.66	0.16	344.67	0	4.04
Taiwan Smart(40)-E01	6.3	1986	0.21	0.57	0.37	0.08	308.39	55.96	57.25
Northridge-Newhall.Fire Sta	6.7	1994	0.59	1.25	0.97	0.34	269.14	3.16	5.92
Loma Prieta-Gilroy Array#3	6.9	1989	0.56	0.46	0.45	0.24	349.85	12.23	12.82
Whittier Narrows- Dam Upstream	6.0	1987	0.32	0.13	0.15	0.03	298.68	2.6	14.73
Northridge-Sylmar.Converter Sta	6.7	1994	0.92	1.69	1.16	0.39	251.24	0	5.35
Whittier Narrows-Bell Gardens Jaboneria	6.0	1987	0.23	0.48	0.28	0.05	267.13	10.31	17.79
Northridge-Canoga Park.Topanga Can	6.7	1994	0.39	0.71	0.63	0.13	267.49	0	14.7
Chi Chi Taiwan03-TCU065	6.2	1999	0.35	0.50	0.27	0.12	305.85	25.17	26.05
Chi Chi Taiwan06-CHY036	6.3	1999	0.20	0.23	0.17	0.09	233.14	45.1	46.19
Northridge01-Tarzana-Cedar Hill A	6.7	1994	1.78	1.42	1.10	0.32	257.21	0.37	15.6

Table 3  
The list of selected ground motions with strike-slip faulting mechanism

Record	Magnitude ( $M_w$ )	Year	PGA(g)	$S_a(T_1)$ (g)	PGV( $\frac{m}{s}$ )	PGD(m)	$v_{s30}$ ( $\frac{m}{s}$ )	$R_{jb}$ (Km)	$R_{RUP}$ (Km)
Landers-Baker Fire Station	7.3	1992	0.11	0.10	0.11	0.08	324.62	87.94	87.94
Parkfield-Cholame Shandon Array#8	6.2	1966	0.27	0.18	0.11	0.05	256.82	12.9	12.9
Imperial Valley-Bonds Corner	6.5	1979	0.78	1.08	0.47	0.20	223.03	0.44	2.66
Trinidad-Rio Dell Overpass E Ground	7.2	1980	0.16	0.22	0.10	0.04	311.75	76.06	76.26
Chalfant Valley02-Bishop LADWP South St	6.2	1986	0.25	0.29	0.20	0.08	303.47	14.38	17.17
Parkfield 02 CA-Parkfield Fault Zone 1	6.0	2004	0.83	1.27	0.81	0.11	178.27	0.02	2.51
Morgan Hill-Hollister City Hall	6.2	1984	0.07	0.25	0.10	0.05	198.77	30.76	30.76
Imperial Valley06-Compuertas	6.5	1979	0.19	0.15	0.14	0.04	259.86	13.52	15.3
Darfield New Zealand-Kaiapoi North School	7.0	2010	0.36	0.39	0.40	0.34	255	30.53	30.53
Parkfield 02 CA-Parkfield Fault Zone 15	6.0	2004	0.23	0.38	0.23	0.06	307.59	0.8	2.67
Imperial Valley 06-El Centro Array #8	6.5	1979	0.61	0.49	0.54	0.42	206.08	3.86	3.86
Superstition Hills 02-Parachute Test Site	6.5	1987	0.43	0.88	1.34	0.46	348.69	0.95	0.95
Victoria Mexico-SAHOP Flores	6.3	1980	0.10	0.11	0.09	0.02	259.59	39.1	39.3
Morgan Hill-Gilroy Array #4	6.2	1984	0.35	0.25	0.19	0.04	221.78	11.53	11.54
Parkfield 02 CA-Parkfield Cholame 2WA	6.0	2004	0.62	1.09	0.64	0.12	173.02	1.63	3.01
Parkfield-Cholame Shandon Array #5	6.2	1966	0.44	0.23	0.25	0.06	289.56	9.58	9.58
Parkfield 02 CA-Parkfield Cholame 3W	6.0	2004	0.58	0.62	0.38	0.07	230.57	2.55	3.63
Kocaeli-Yarimca	7.5	1999	0.32	0.58	0.72	0.62	297	1.38	4.83
Parkfield 02 CA-Parkfield Fault Zone 14	6.0	2004	1.31	1.13	0.83	0.17	246.07	8.46	8.81
Chalfant Valley-Zack Brothers Ranch	6.2	1986	0.45	1.13	0.45	0.09	316.19	6.44	7.58

Choosing the suitable intensity measure (IM) is a crucial step in fragility analysis. Researchers have suggested various methods for selecting a proper IM. One of these methods is the efficiency analysis by Buratti [66], which defines an IM as efficient if it can minimize the variation in the structural response for a given IM value. Buratti and Tavano [67] conducted a study where they performed a linear statistical regression between the radial displacement responses of the tank model they investigated and the intensity measures of peak ground acceleration

(PGA), peak ground velocity (PGV), peak ground displacement (PGD), and spectral acceleration at the first natural period PSA, based on the cloud analysis. They concluded that PGD was an efficient IM for fragility analysis. To select the appropriate IM for vulnerability assessments in the present study, a linear statistical regression was conducted between the logarithm of the maximum recorded strain and various IMs, including PGA, PGV, PGD, and spectral acceleration of the fundamental period ( $S_A(T_1)$ ), where  $T_1 = 0.86s$ . (refer to Fig. 4). The

correlation between these two sets of parameters was evaluated using the coefficient of determination ( $R^2$ ) to select the most suitable IM. The coefficient of

determination values for the different IMs are presented in Table 4.

Table 4  
The coefficient of determination for different IM parameters

Intensity measure	The coefficient of determination ( $R^2$ )
PGA	0.67
PGV	0.58
$S_a(T_1)$	0.45
PGD	0.33

Compared to other IMs, the logarithmic peak strain responses have a higher coefficient of determination to the logarithmic PGA, as the results indicate. However, despite this, the PGA is commonly used in presenting fragility curves. Conversely, when studying bridges, it is advisable to use the spectral acceleration of the fundamental period of the bridge. Consequently, in the current study, fragility curves were developed using both the PGA and  $S_A(T_1)$  as selected IMs.

study represented each value of the IM with an earthquake record, and the earthquake record was not scaled. As a result, elevating the level of IM may not necessarily lead to increased damage. Therefore, the suggested maximum likelihood method is beneficial in optimizing the outcomes of fragility analysis. The equation for this method is presented below:

$$\left\{ \hat{\theta}, \hat{\beta} \right\} = \arg \max_{\theta, \beta} \sum_{j=1}^m \left\{ \ln \binom{n_j}{z_j} + z_j \ln \Phi \left( \frac{\ln \left( \frac{x_j}{\theta} \right)}{\beta} \right) + (n_j - z_j) \ln \left( 1 - \Phi \left( \frac{\ln \left( \frac{x_j}{\theta} \right)}{\beta} \right) \right) \right\} \quad (3)$$

In this relationship,  $\theta$  and  $\beta$  represent the initial values of the mean and standard deviation of the lognormal CDF. The variable  $z_j$  denotes the number of observed cases among  $n_j$  ground motions with the  $IM = x_j$  that have exceeded the limit state. Additionally, the output values of the equation, represented by  $\hat{\theta}$  and  $\hat{\beta}$ , are used to replace the initial values of the lognormal CDF to develop the fragility curve.

#### 4. Fragility Analysis

In this study, fragility curves were developed based on earthquake-scour multi-hazard analyses. These curves were calculated for two different IMs and three levels of damage: minor, moderate, and extensive. Then the results were compared according to the different scour scenarios.

##### 4.1. Comparing the Fragility Analyses of Uniform and Non-Uniform Scenarios

The study considered all the random depths from the Latin hypercube sampling technique as different patterns in two scenarios, which included both even and uneven depths in different foundations. The fragility curves for two conditions, one with uniform and the other with non-uniform characteristics are depicted in Fig. 5.

The findings indicate that, in all three limit states and for both IMs, the probability of exceeding the

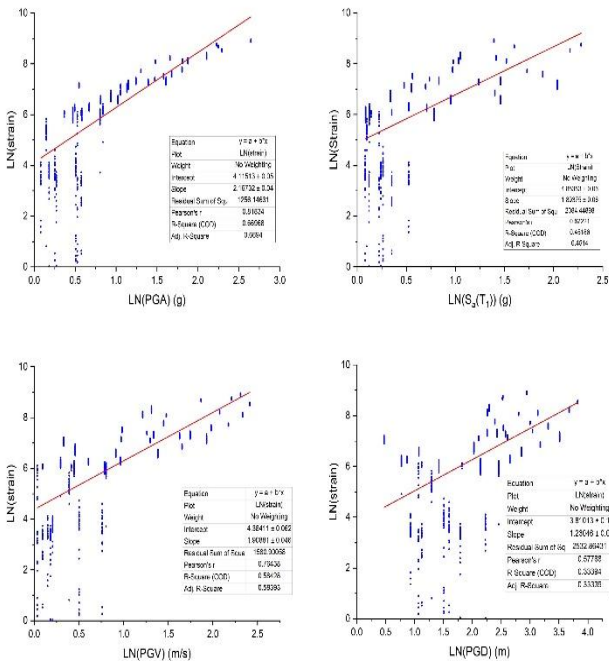


Fig. 4. Logarithmic peak strain versus logarithmic PGA, PGV, PGD and  $S_A(T_1)$ : a linear regression analysis

The study conducted fragility analyses by utilizing the lognormal cumulative distribution function (CDF) and employing the maximum likelihood method suggested by Baker [68]. Unlike the IDA method, the structural analysis method used in this



limit state is higher in the uniform scenario. Although the difference between the two scenarios is less in the minor limit state, the results demonstrate that the difference between the probability of uniform and non-uniform models in the fragility curves of the moderate and extensive limit states, as measured by PGA, is as high as 9%.

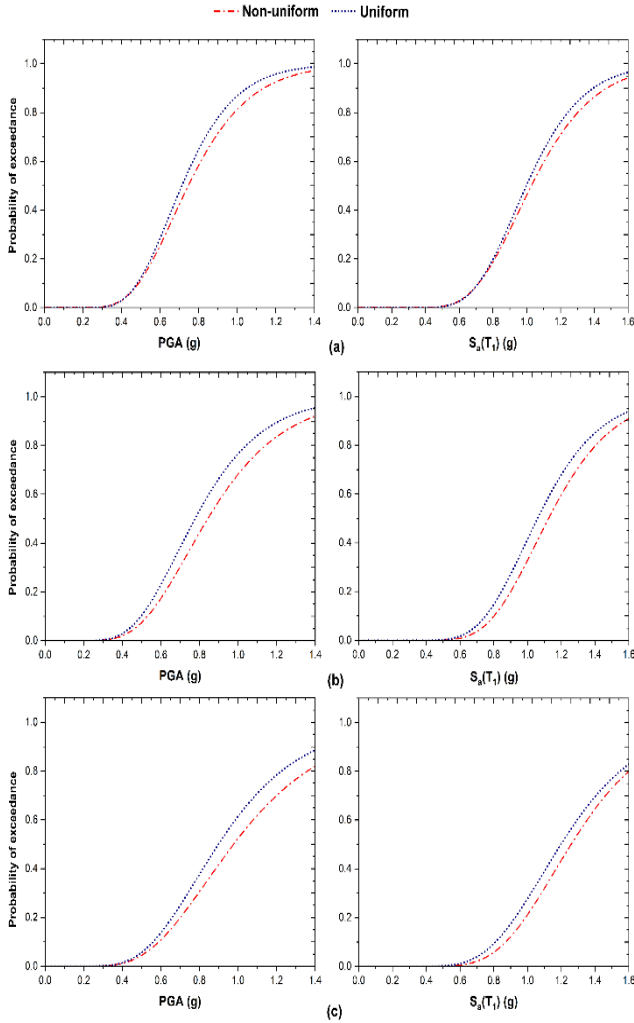


Fig. 5. The difference between the fragility curves for uniform and non-uniform scour scenarios across (a) minor, (b) moderate, and (c) extensive limit states

#### 4.2. Fragility Curves for Patterns with Uniform Half and Maximum Scoured Piers

The study made a pattern called uniformly half-scoured (UHS), where all foundations had a scour depth of two meters, to examine the influence of scour depth on fragility curves. This pattern was then compared to the uniformly maximum credible scoured pattern (UMCS), where all foundations were washed out to a depth of four meters (refer to Fig. 6). The results indicate the probability of exceeding all

three limit states is higher for the UMCS pattern. Although the effect of depth in the uniform scenario is less noticeable in the first two limit states, it is significant in the extensive limit state. At PGA=0.85g, the probability of exceeding the extensive limit state increases by 23% when the pattern changes from the UHS to the UMCS.

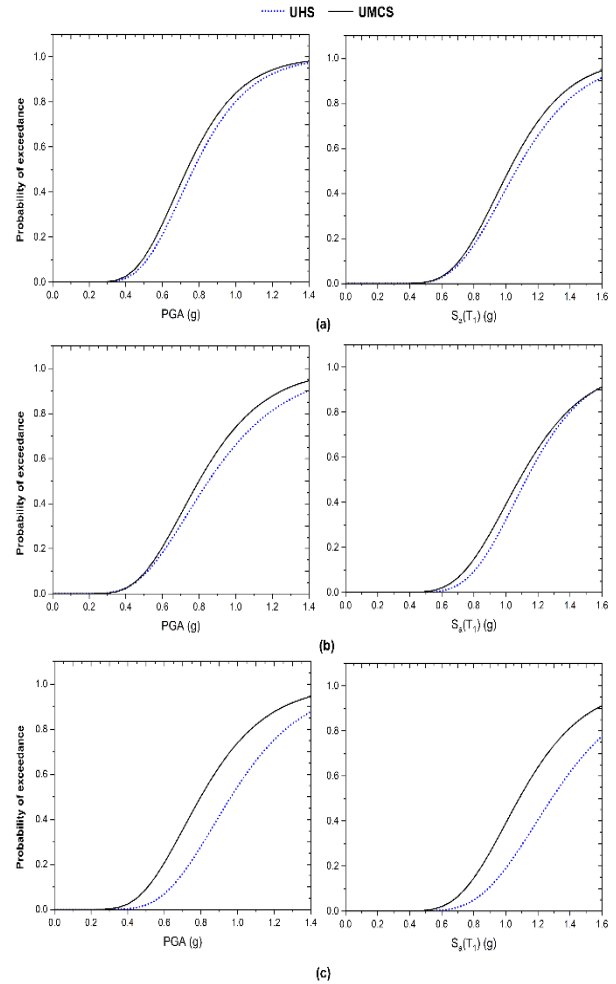


Fig. 6. The difference between the fragility curves for UHS and UMCS scour patterns across (a) minor, (b) moderate, and (c) extensive limit states

#### 4.3. Fragility Curves for Patterns with Non-uniform Half and Maximum Scoured Pier(s)

Several non-uniform random patterns have at least one foundation with the maximum scoured depth. This scenario is called non-uniform containing maximum credible scoured foundation(s) (NCMCS). Another scenario is non-uniform containing half-scoured foundation(s) (NCHS), which has at least one pier with a 2 m scour depth in random patterns.

Fig. 7 shows the comparison between these two scenarios.

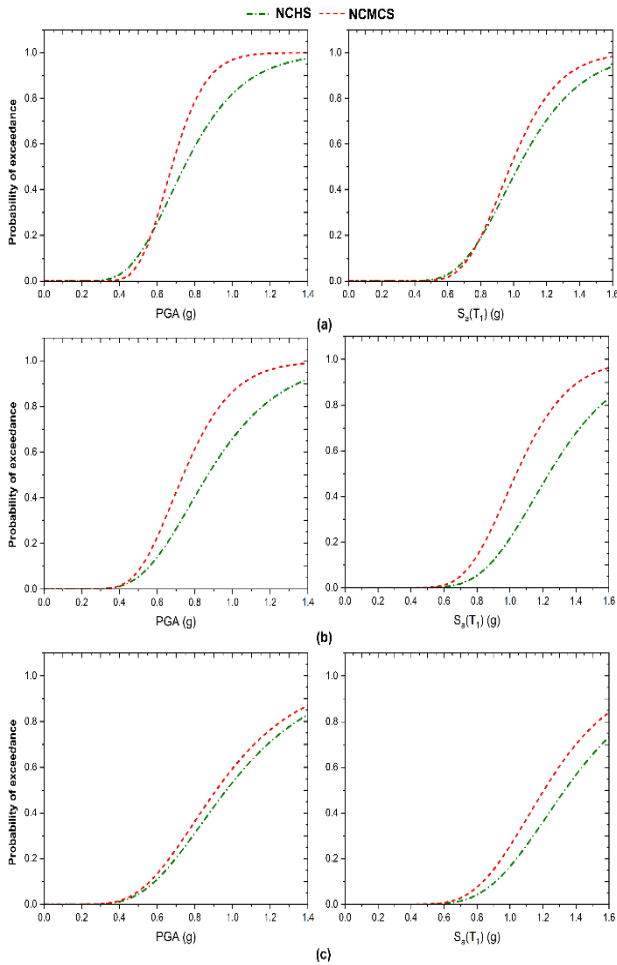


Fig. 7. The difference between the fragility curves for NCMCS and NCHS scour scenarios across (a) minor, (b) moderate, and (c) extensive limit states

There are differences in the probability of exceeding between the two scenarios in all three damage states. In the minor limit state and when PGA is equal to 0.9g, the NCMCS has increased the probability of exceeding by a maximum of 20% compared to the other scenario. In the moderate limit state, for both IMs comprising PGA and  $S_a(T_1)$ , changing the scenarios has resulted in a maximum increase of 22% and 27% in the probability of exceeding, respectively.

Overall, it can be inferred that the impact of the depth of scour on the susceptibility of the examined bridge model is contingent upon the type of scour scenario, which may be either uniform or non-uniform, as well as the particular state of damage that is being studied.

#### 4.4. Comparing the Fragility Analyses of NCMCS and UMCS Scenarios

To compare the scenarios of uniform and non-uniform scour, we have also compared critical patterns in these two scenarios. The fragility curves NCMCS and UMCS that were developed have been compared with each other, as shown in Fig 8.

The results indicate that until the PGA gets to about 0.6g, the UMCS pattern has a higher probability of exceeding the minor and moderate limit states. After that point, the NCMCS scenario has a higher probability of exceeding. It differs from the extensive limit state, in which consistently the UMCS pattern stays at higher levels for the whole range of IM.

In the minor and moderate limit states, the disparity between the two fragility curves in measure of PGA reaches a maximum of 13%. However, the maximum difference between the two fragility curves for the same limit states, when measured in terms of spectral acceleration of the fundamental period, is 9%.

In the extensive, as opposed to the two initial limit states, when considering higher intensity measures, the probability of exceeding both intensity measures simultaneously shows a maximum increase of approximately 15% for the UMCS pattern.

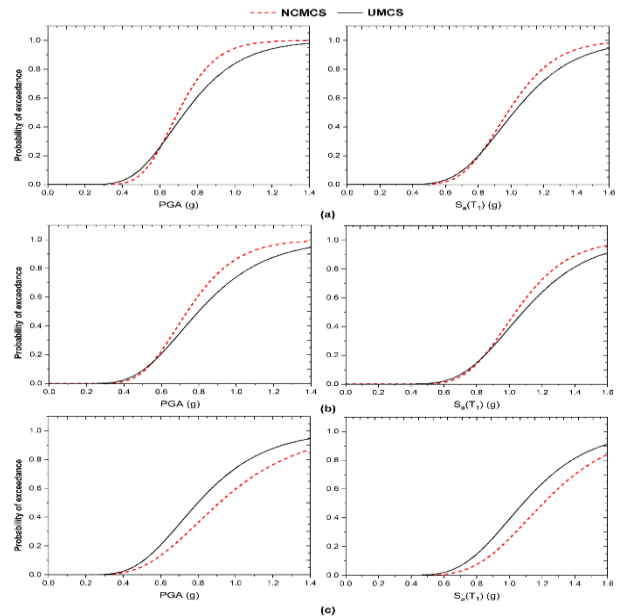


Fig. 8. The difference between the fragility curves for UMCS and NCMCS scour scenarios across (a) minor, (b) moderate, and (c) extensive limit states

## 5. Conclusions

Numerous research studies have been carried out to investigate the vulnerability of bridges to earthquakes. However, there is a shortcoming of adequate research on multi-hazard assessments, which encompass scouring and earthquakes, to obtain more comprehensive outcomes. The analysis results depend on various factors, such as the different bridge classes, hydraulic data of rivers, precipitation levels, probabilistic flood assessments, geometric features of bridge components, soil type, and other factors. Hence, there are numerous uncertainties involved in analyzing the bridge model. One of the cases that has been specifically examined in this study pertains to the non-uniformity of scour depth in various foundations, which is caused by the random formation of erosion cavities. The study employed Monte Carlo and Latin hypercube sampling methods to investigate this. Furthermore, the research evaluated uniform patterns by placing the same random scour depths in three different bridge piers. The findings indicate that in all three limit states investigated, the uniform scenario has a higher probability of exceeding than the non-uniform one.

In the investigation of critical erosion patterns, the results reveal that the UMCS pattern with the maximum scour depth (4 meters deep) is not necessarily the most vulnerable in all cases. Only in the extensive limit state, this pattern has a higher probability of exceeding than the NCMCS scenario. For the minor and moderate limit states, the NCMCS scenario has a higher chance of exceeding.

To assess the impact of scour depth, a pattern known as UHS was established, which resulted in an equal scour depth of 2 meters in all three piers of the bridge. The findings indicate that in the minor and moderate limit states, although the fragility curves are at lower probability levels than the UMCS pattern, there is not a significant difference between these two curves. However, in the extensive limit state, the UMCS is positioned at a higher level, and the maximum difference between the two fragility curves in the PGA measure is 23%.

For the non-uniform scouring case, the study compared the NCHS scenario with half-scoured pier(s) to the NCMCS scenario. The vulnerability assessment of these scenarios also indicated a 20% and 22% increase in the probability of exceeding the minor and moderate limit states for the PGA measure.

It is necessary to acknowledge that the model geometry plays a critical role in determining the results of the vulnerability assessments. The findings of this study are applicable solely to the particular class of bridge that was examined, and any variations in geometry or conditions would necessitate a fresh analysis.

## References

- [1] Richardson, E. V., HUBER, F. W. (1991). Evaluation of Bridge Vulnerability to Hydraulic Forces, Stream Instability. Transportation Research Record, 1290, 25.
- [2] May, R. W. P., Ackers, J. C., Kirby, A. M. (2002). Manual on scour at bridges and other hydraulic structures (Vol. 551), London, UK: Ciria.
- [3] Wang, Z., Padgett, J. E., Dueñas-Osorio, L. (2014). Risk-consistent calibration of load factors for the design of reinforced concrete bridges under the combined effects of earthquake and scour hazards. Engineering Structures, 79, 86-95.
- [4] Hayes, D. C., Drummond, F. E. (1995). Use of fathometers and electrical-conductivity probes to monitor riverbed scour at bridge piers (Vol. 94, No. 4164). US Department of the Interior, US Geological Survey.
- [5] Lagasse, P. F. (1997). Instrumentation for measuring scour at bridge piers and abutments (No. 21). Transportation Research Board.
- [6] Yankielun, N. E., Zabilansky, L. (1999). Laboratory investigation of time-domain reflectometry system for monitoring bridge scour. Journal of Hydraulic engineering, 125(12), 1279-1284.
- [7] Hunt, B. E. (2009). Monitoring scour critical bridges (Vol. 396). Transportation Research Board.
- [8] Priestley, M. J. N. (1988). The whittier narrows, California earthquake of October 1, 1987—damage to the I-5/I-605 separator. Earthquake Spectra, 4(2), 389-405.
- [9] Mitchell, D., Bruneau, M., Saatcioglu, M., Williams, M., Anderson, D., Sexsmith, R. (1995). Performance of bridges in the 1994 Northridge earthquake. Canadian Journal of Civil Engineering, 22(2), 415-427.
- [10] Chang, K. C., Chang, D. W., Tsai, M. H., Sung, Y. C. (2000). Seismic Performance of Highway Bridges.

- [11] Lehman, D., Moehle, J., Mahin, S., Calderone, A., Henry, L. (2004). Experimental evaluation of the seismic performance of reinforced concrete bridge columns. *Journal of Structural Engineering*, 130(6), 869-879.
- [12] Saiidi, M. S., Vosooghi, A., Nelson, R. B. (2013). Shake-table studies of a four-span reinforced concrete bridge. *Journal of Structural Engineering*, 139(8), 1352-1361.
- [13] Su, J., Wang, J., Li, Z., Liang, X. (2019). Effect of reinforcement grade and concrete strength on seismic performance of reinforced concrete bridge piers. *Engineering Structures*, 198, 109512.
- [14] Tesfamariam, S., Goda, K. (Eds.). (2013). *Handbook of seismic risk analysis and management of civil infrastructure systems*. Elsevier.
- [15] Kim, H., Sim, S. H., Lee, J., Lee, Y. J., Kim, J. M. (2017). Flood fragility analysis for bridges with multiple failure modes. *Advances in Mechanical Engineering*, 9(3), 1687814017696415.
- [16] Anisha, A., Jacob, A., Davis, R., Mangalathu, S. (2022). Fragility functions for highway RC bridge under various flood scenarios. *Engineering Structures*, 260, 114244.
- [17] Ahamed, T., Duan, J. G., Jo, H. (2021). Flood-fragility analysis of instream bridges—consideration of flow hydraulics, geotechnical uncertainties, and variable scour depth. *Structure and Infrastructure Engineering*, 17(11), 1494-1507.
- [18] Nielson, B. G. (2005) Analytical fragility curves for highway bridges in moderate seismic zones. Georgia Institute of Technology.
- [19] Feng, M. Q., Shinozuka, M., Kim, H. K., Kim, S. H. (2000) Statistical analysis of fragility curves.
- [20] Hwang, H., Jernigan, J. B., Lin, Y. W. (2000). Evaluation of seismic damage to Memphis bridges and highway systems. *Journal of Bridge Engineering*, 5(4), 322-330.
- [21] Choi, E., DesRoches, R., Nielson, B. (2004). Seismic fragility of typical bridges in moderate seismic zones. *Engineering structures*, 26(2), 187-199.
- [22] Nielson, B. G., DesRoches, R. (2007) Analytical seismic fragility curves for typical bridges in the central and southeastern United States. *Earthquake spectra*, 23(3), 615-633.
- [23] Ramanathan, K., DesRoches, R., Padgett, J. E. (2012). A comparison of pre-and post-seismic design considerations in moderate seismic zones through the fragility assessment of multi-span bridge classes. *Engineering Structures*, 45, 559-573.
- [24] Chen, X. (2020). System fragility assessment of tall-pier bridges subjected to near-fault ground motions. *Journal of Bridge Engineering*, 25(3), 04019143.
- [25] Decò, A., Frangopol, D. M. (2011). Risk assessment of highway bridges under multiple hazards. *Journal of Risk Research*, 14(9), 1057-1089.
- [26] Kameshwar, S., Padgett, J. E. (2014). Multi-hazard risk assessment of highway bridges subjected to earthquake and hurricane hazards. *Engineering Structures*, 78, 154-166.
- [27] Fan, W., Sun, Y., Yang, C., Sun, W., He, Y. (2020). Assessing the response and fragility of concrete bridges under multi-hazard effect of vessel impact and corrosion. *Engineering structures*, 225, 111279.
- [28] Zhou, M., Yin, S., Zhu, G., Fu, J. (2022). Seismic Performance Evaluation of Highway Bridges under Scour and Chloride Ion Corrosion. *Applied Sciences*, 12(13), 6680.
- [29] Dong, Y., Frangopol, D. M., Saydam, D. (2013). Time-variant sustainability assessment of seismically vulnerable bridges subjected to multiple hazards. *Earthquake Engineering & Structural Dynamics*, 42(10), 1451-1467.
- [30] Fioklou, A., Alipour, A. (2014). Seismic behavior of bridges with deep foundations under effects of scouring. In *Structures Congress 2014* (pp. 313-323).
- [31] Wang, Z., Dueñas-Osorio, L., Padgett, J. E. (2014). Influence of scour effects on the seismic response of reinforced concrete bridges. *Engineering structures*, 76, 202-214.
- [32] Song, S. T., Hu, T. F., Chiou, D. J. (2022). Influence of riverbed scour on the performance of bridges subjected to lateral seismic loads. *Journal of Earthquake Engineering*, 26(5), 2251-2282.
- [33] Fioklou, A., Alipour, A., (2019). Significance of non-uniform scour on the seismic performance of bridges. *Structure and Infrastructure Engineering*, 15(6), 822-836.
- [34] Alipour, A., Shafei, B. (2012). Performance assessment of highway bridges under earthquake and scour effects. In *Proceedings of the*

- conference on earthquake engineering (pp. 24-28).
- [35] Alipour, A., Shafei, B., Shinozuka, M. (2013). Reliability-based calibration of load and resistance factors for design of RC bridges under multiple extreme events: Scour and earthquake. *Journal of Bridge Engineering*, 18(5), 362-371.
- [36] Guo, X., Wu, Y., Guo, Y. (2016). Time-dependent seismic fragility analysis of bridge systems under scour hazard and earthquake loads. *Engineering Structures*, 121, 52-60.
- [37] Richardson, E. V., Davis, S. R. (1995) Evaluating scour at bridges (No. HEC 18). United States, Federal Highway Administration, Office of Technology Applications.
- [38] Froehlich, D. C. (1988). Analysis of onsite measurements of scour at piers. In *Hydraulic engineering: proceedings of the 1988 national conference on hydraulic engineering* (pp. 534-539).
- [39] Melville, B. W. (1997). Pier and abutment scour: integrated approach. *Journal of hydraulic Engineering*, 123(2), 125-136.
- [40] Coleman, S. E. (2005). Clearwater local scour at complex piers. *Journal of Hydraulic Engineering*, 131(4), 330-334.
- [41] Johnson, P. A., Dock, D. A. (1998). Probabilistic bridge scour estimates. *Journal of Hydraulic Engineering*, 124(7), 750-754.
- [42] Banerjee, S., Ganesh Prasad, G. (2013). Seismic risk assessment of reinforced concrete bridges in flood-prone regions. *Structure and Infrastructure Engineering*, 9(9), 952-968.
- [43] American Association of State Highway and Transportation Officials (AASHTO). (2020). *LRFD Bridge Design Specifications*, 9th ed. AASHTO LRFD BDS-9(2020). Washington, DC:
- [44] Mosleh, A., Sepahvand, K., Varum, H., Jara, J., Razzaghi, M. S., Marburg, S. (2018). Stochastic collocation-based nonlinear analysis of concrete bridges with uncertain parameters. *Structure and Infrastructure Engineering*, 14(10), 1324-1338.
- [45] Mazzoni S, McKenna F, Scott M. H., Fenves, G. L. (2006). *OpenSees Command Language Manual*. Pacific Earthquake Engineering Research (PEER) Center, University of California, Berkeley, CA, USA.
- [46] Mander, J. B., Priestley, M. J., Park, R. (1988). Theoretical stress-strain model for confined concrete. *Journal of structural engineering*, 114(8), 1804-1826.
- [47] Simon, J., Vigh, L. G. (2016). Seismic fragility assessment of integral precast multi-span bridges in areas of moderate seismicity. *Bulletin of Earthquake Engineering*, 14, 3125-3150.
- [48] Megally, S. H., Silva, P. F., Seible, F. (2001). Seismic response of sacrificial shear keys in bridge abutments. *SSRP*, 23.
- [49] Bozorgzadeh, A., Megally, S. H., Ashford, S., Restrepo, J. I. (2007). Seismic response of sacrificial exterior shear keys in bridge abutments. *Ssrp*, 4, 14.
- [50] California Department of Transportation (CALTRANS). (2004). *Seismic design criteria. Version 1.3*, California Dept. of Transportation, Sacramento, CA.
- [51] Muthukumar, S. (2003). A contact element approach with hysteresis damping for the analysis and design of pounding in bridges. Georgia Institute of Technology.
- [52] American Petroleum Institute (API). (1993). *Recommended practice for planning, designing, and constructing fixed offshore platforms. vol. 2*. American Petroleum Institute;
- [53] Mosher, R. L. (1984). *Load-transfer Criteria for Numerical Analysis of Axially Loaded Piles in Sand: Part 1: Load-transfer Criteria* (p. 0390). Vicksburg, MS: US Army Engineer Waterways Experiment Station.
- [54] Kulhawy, F. H. (1991). Drilled shaft foundations. In *Foundation engineering handbook* (pp. 537-552). Boston, MA: Springer US.
- [55] Zhang, L., Silva, F., Grimala, R. (2005). Ultimate lateral resistance to piles in cohesionless soils. *Journal of Geotechnical and Geoenvironmental Engineering*, 131(1), 78-83.
- [56] Vijavergiya, V. N. (1977) Load-movement characteristics of piles. In *4th Symp. of Waterway, Port, Coastal and Ocean Div.*, ASCE (Vol. 2, pp. 269-284).
- [57] Meyerhof, G. G. (1976). Bearing capacity and settlement of pile foundations. *Journal of the Geotechnical Engineering Division*, 102(3), 197-228.
- [58] Das, B. M., Sivakugan, N. (2018). *Principles of foundation engineering*. Cengage learning.
- [59] Ramanathan, K. N. (2012). Next generation seismic fragility curves for California bridges incorporating the evolution in seismic design philosophy. Georgia Institute of Technology.

- [60] Priestley, M. N., Seible, F., Calvi, G. M. (1996). Seismic design and retrofit of bridges. John Wiley & Sons.
- [61] Mander, J. B., Basöz, N. (1999). Seismic fragility curve theory for highway bridges. In Optimizing post-earthquake lifeline system reliability (pp. 31-40). ASCE.
- [62] Kowalsky, M. J. (2000). Deformation limit states for circular reinforced concrete bridge columns. *Journal of Structural Engineering*, 126(8), 869-878.
- [63] Hosseini, A. R. M., Razzaghi, M. S., Shamskia, N. (2023). Probabilistic seismic safety assessment of bridges with random pier scouring. *Proceedings of the Institution of Civil Engineers-Structures and Buildings*, 1-18.
- [64] Miano, A., Jalayer, F., Ebrahimian, H., Prota, A. (2019). Nonlinear dynamic analysis procedure with limited number of analyses and scaling. In *Proceedings of the 7th ECCOMAS Thematic Conference on Computational Methods in Structural Dynamics and Earthquake Engineering (COMPdyn)*, Crete, Greece (pp. 24-26).
- [65] Contiguglia, C. P., Pelle, A., Briseghella, B., Nuti, C. (2022). IMPA versus Cloud Analysis and IDA: different methods to evaluate structural seismic fragility. *Applied Sciences*, 12(7), 3687.
- [66] Buratti, N. (2012). A comparison of the performances of various ground-motion intensity measures. In *Proceedings of the 15th world conference on earthquake engineering*, Lisbon, Portugal (pp. 24-28).
- [67] Buratti, N., Tavano, M. (2014). Dynamic buckling and seismic fragility of anchored steel tanks by the added mass method. *Earthquake Engineering & Structural Dynamics*, 43(1), 1-21.
- [68] Baker, J. W. (2015). Efficient analytical fragility function fitting using dynamic structural analysis. *Earthquake Spectra*, 31(1), 579-599.